# Inferring Global Synchrony from Local Symbolic Dynamics

Sarika Jalan, Fatihcan M. Atay, Jürgen Jost

*Max Planck Institute for Mathematics in the Sciences, 04103 Leipzig, Germany*

**Abstract**

We present a method based on symbolic dynamics for the detection of synchronization in networks of coupled oscillators. The symbolic dynamics are defined using special partitions of the phase space which prevent the occurrence of certain symbol sequences related to the characteristics of the dynamics. These partitions are chosen to best distinguish chaotic (but deterministic) dynamics from random ones in the uncoupled case. In the coupled case, they allow for a rapid detection of qualitative types of emerging collective dynamics. As a direct application, we can detect synchronization of coupled chaotic dynamics on networks from a single randomly selected node by comparing the transition probabilities with those of the uncoupled function. The method utilizes a relatively short time series of measurements and hence is computationally very fast. Furthermore, it is robust against parameter uncertainties, is independent of the network size, and does not require knowledge of the connection structure. We present our method for the one-dimensional logistic map, the two-dimensional Hénon map, and the three-dimensional Lorenz oscillator as local dynamical function, and for various different coupling structures.

*Key words:* Synchronization, coupled oscillators, symbolic dynamics, neural network

## 1 Introduction

Synchronization is the prototype of an emerging system level behaviour of interacting dynamical units. This behaviour, in large ensembles of coupled dynamical units, is studied in many different fields [1,2], describing synchronous behaviour in various natural and artificial systems such as Belousov-Zhabotinsky

*Email addresses:* sjalan@mis.mpg.de (Sarika Jalan), atay@member.ams.org (Fatihcan M. Atay), jjost@mis.mpg.de (Jürgen Jost).

reaction [3], neuronal activities in different cortical regions of cat [4], brain signals during epileptic seizures [5,6], technical systems such as power grids to achieve secure communication [7], climate behaviour such as solar forcing of Indian monsoon [8] etc. Depending on the field, synchronization can be a desired or undesirable behaviour. Detection of synchronization in extended systems from local measurements has important applications. For example, during anaesthesia, it is found that the dynamical activity passes reversibly through a sequence of different cardiorespiratory synchronized states as the anaesthesia level changes, and thus the synchronization state may be used to characterize the depth of anaesthesia [9]. Certain pathologies in the neural system, such as epileptic seizures, manifest themselves by synchronized brain signals [5], and there is some evidence that they can be predicted by changing levels of synchronization [6]. It is thus of interest to be able to determine different levels of synchronization in a brain area from local measurements, such as EEG recordings. So far the methods used to detect synchronization are based on cross correlation function analysis. For multivariate time series, this relies on the proper embedding of the phase space. Mutual false nearest neighbour or mixed state embedding methods are also used to detect synchronization. All these methods have their practical limitations and are very difficult to implement when the data are noisy and of limited length [10,11]. Here, we describe a new method to detect synchronization based on symbolic dynamics. Symbolic dynamics is a fundamental tool for describing a complicated time evolution of a chaotic dynamical system [12,13]. Instead of representing a trajectory by an infinite sequences of numbers one watches the alternation of symbols. In doing so one 'loses' a great amount of information but some invariant, robust properties of the dynamics may be kept. A good symbolic dynamics representation crucially depends on the partition of phase space [14,15].

We define symbolic dynamics based on specific partitions which prevent the occurrence of certain symbolic sequences characteristic of the dynamical function. This partition leads to the maximal difference in the permutation entropy [16] of a chaotic and the corresponding random system [17]. The symbolic dynamics defined by such partition has several practical applications [17,18]. One such application is the detection of global synchronization in coupled chaotic systems. The synchronized state is detected by simply observing the complete absence or at least low frequency of particular symbol sequences. The method uses a very short time series and is hence computationally very fast. Also, because it compares the symbol sequence of one single unit in the network with some model behaviour, it does not depend on the size of the network and is robust against external noise.

## 2 Definition of Symbolic Dynamics

We consider a dynamical system

$$\dot{\mathbf{x}}(t) = \mathbf{F}(\mathbf{x}(t)) \tag{1}$$

where $\mathbf{x} = (x^{(1)}, x^{(2)}, \ldots, x^{(k)}) \in \mathbb{R}^k$, $\mathbf{F}(\mathbf{x}) = (F^{(1)}(\mathbf{x}), F^{(2)}(\mathbf{x}), \ldots, F^{(k)}(\mathbf{x}))$ is a $k$-dimensional vector function of $\mathbf{x}$, and $\dot{\mathbf{x}}$ denotes the time derivative $d\mathbf{x}/dt$. Let $S \subset \mathbb{R}^k$ be an invariant set for (1), and $\{S_i : i = 1, \ldots, m\}$ be a partition of $S$, i.e., a collection of mutually disjoint and nonempty subsets satisfying $\cup_{i=1}^{m} S_i = S$. The symbolic dynamics corresponding to (1) is the sequence of symbols $\{\ldots, s_{t-\triangle t}, s_t, s_{t+\triangle t}, \ldots\}$ where $s_t = i$ if $\mathbf{x}(t) \in S_i$.

## 3 Choice of the Partition

For our applications, a judicious choice of partition is crucial. Suppose the scalar $x^{(n)}$, $1 \leq n \leq k$, is available for measurement. For a given threshold value $x^* \in \mathbb{R}$, define the sets

$$S_1 = \{\mathbf{x} \in S : x^{(n)} < x^*\}$$
$$S_2 = \{\mathbf{x} \in S : x^{(n)} \geq x^*\}$$

The value of $x^{(n)}$ can be chosen to make the sets $S_1, S_2$ nonempty, in which case they form a non-trivial partition of $S$. For this special partition, we use the two-symbol dynamics generated by

$$s_t = \begin{cases} \alpha \text{ if } x^{(n)}(t) < x^* \\ \beta \text{ if } x^{(n)}(t) \geq x^*. \end{cases} \tag{3}$$

The symbolic dynamics depends only on the measurements $x^{(n)}$, yielding a sequence of symbols determined by whether a measured value exceeds the threshold $x^*$ or not. Essentially any choice of the threshold $x^*$ will yield a non-generating partition. We say that the set $S_i$ *avoids* $S_j$ if

$$x(t) \in S_i \Rightarrow x(t + \triangle t) \notin S_j \tag{4}$$

We look for a partition which contains avoiding sets. The significance is that if $S_i$ avoids $S_j$, then the symbolic dynamics cannot contain the symbol sequence $ij$, and we say that the transition $i \to j$ is *forbidden*. The essence of our symbolic dynamics is based on choosing a partition where (4) holds for one or more sets in the partition. We estimate the transition probability $P(i, j)$

by the ratio $\sum_t n(s_t = i, s_{t+\triangle t} = j)/\sum_t n(s_t = i)$, where $n$ is the count of the number of occurrences.

For practical calculations using short time series, choice of $x^*$ becomes important. The choice should make certain transition probabilities very small. Clearly, increasing the threshold decreases the probability of occurrence of the repeated sequence $\beta\beta$. However, it also decreases the probability of observing the single symbol $\beta$, making it difficult to work with short time series. Hence, the choice of the threshold is a compromise between these two effects. We use the natural density defined by the data to choose a threshold. In the following section we will present the method by taking examples of two different maps. The method can simply be extended for the continuous systems, where $\triangle t$ has to be chosen such that for the appropriate $x^*$, we get certain transition probabilities zero. Note that this can always be done if $\triangle t$ is chosen sufficiently small. However, measurement conditions impose a lower bound on $\triangle t$.

## 4 Coupled dynamics on networks and Global Synchrony

We present the method to detect synchronized chaos in large extended systems. Consider the following coupled oscillator model,

$$\dot{\mathbf{x}}_i(t) = \mathbf{F}(\mathbf{x}_i(t)) + \varepsilon \sum_{j=1}^{N} C_{ij}[g(\mathbf{x_i}(t)) - g(\mathbf{x_j}(t))] \tag{5}$$

where $\mathbf{x_i}(t)$ is the state of the $i$th node at time $t$, $i = 1, \ldots, N$, $C_{ij}$ are the elements of the adjacency matrix $\mathbf{C}$ with value 1 or 0 depending upon whether $i$ and $j$ are connected or not, $\varepsilon \in [0, 1]$ is the coupling strength. The system can exhibit a wide range of behaviour depending upon the local dynamics (1) and coupling structure $\mathbf{C}$, so corresponding symbol sequences observed from a node can vary widely. However, at the synchronized state $x_i(t) = x_j(t)$, for all $i, j$ and $t$, all nodes evolve according to the rule (1). It follows that when the network is synchronized, the symbolic sequence measured from a node will be subject to the same constraints as that generated by (1). And a very easy way of detecting synchronization of the network is simply by choosing a random node and calculating the transition probabilities. If these transition probabilities match with the transition probabilities of the isolated dynamics, this confirms the synchronization.

A discrete version of the equation (5) is

$$\mathbf{x}_i(t+1) = \mathbf{f}(\mathbf{x}_i(t)) + \frac{\varepsilon}{k_i} \sum_{j=1}^{N} C_{ij}\,[g(\mathbf{x}_j(t)) - g(\mathbf{x}_i(t))] \tag{6}$$

where, for simplicity and because this occurs in our subsequent applications, we have used the same function $f$ for the local and the interaction dynamics. $k_i$ is the degree of unit $i$, that is, $\sum_j C_{ij}$. For the discrete dynamical system we can write the criteria for forbidden set (Eq. (4)) as,

$$\mathbf{f}(S_i) \cap S_j = \emptyset. \tag{7}$$

We consider logistic/tent, Hénon maps and Lorenz oscillator as the examples for numerical studies.

## 5 Detection of Synchronization

For detection of global synchrony we compare the transition probabilities of any randomly selected node with the transition probabilities of the isolated function. In the ideal case, we can find a partition that has one or more forbidden sets for the dynamics of an isolated unit. This,in fact, is the case for logistic and tent maps. Therefore, in that case, the situation is rather simple as one has to look for the presence or absence of symbol subsequences which are forbidden in the dynamics of the map. Thus, we first demonstrate our results for the tent map. After that, we turn to the Hénon map and Lorenz attractor as a local dynamical function. Here, one does not have strictly forbidden transitions for the dynamics of the individual map, but our method nevertheless applies rather well.

### *5.1 Synchronization Measures*

In this section we write the measures indicating the global synchrony. First is the variance of the variables over the network, which is given by $\sigma^2 = \left\langle \frac{1}{N-1} \sum_i [x_i(t) - \bar{x}(t)]^2 \right\rangle_t$, where $\bar{x}(t) = \frac{1}{N} \sum_i x_i(t)$ denotes an average over the nodes of the network and $\langle \dots \rangle_t$ denotes an average over time. $\sigma^2$ drops to zero when the whole network is synchronized.

We define our symbolic measure for the synchronization as follows. First we estimate the transition probability $P(i,j)$ by the ratio,

$$P(i,j) = \sum_t n(s_t = i, s_{t+1} = j) / \sum_t n(s_t = i), \tag{8}$$

where $n$ is a count of the number of times of occurrence. The deviation of $P(i,j)$ of any node is defined as

$$\delta^2_{i,j} = \left\langle \frac{1}{m-1} \sum_{k=1}^{m} [P_k(i,j) - \overline{P(i,j)}]^2] \right\rangle, \tag{9}$$

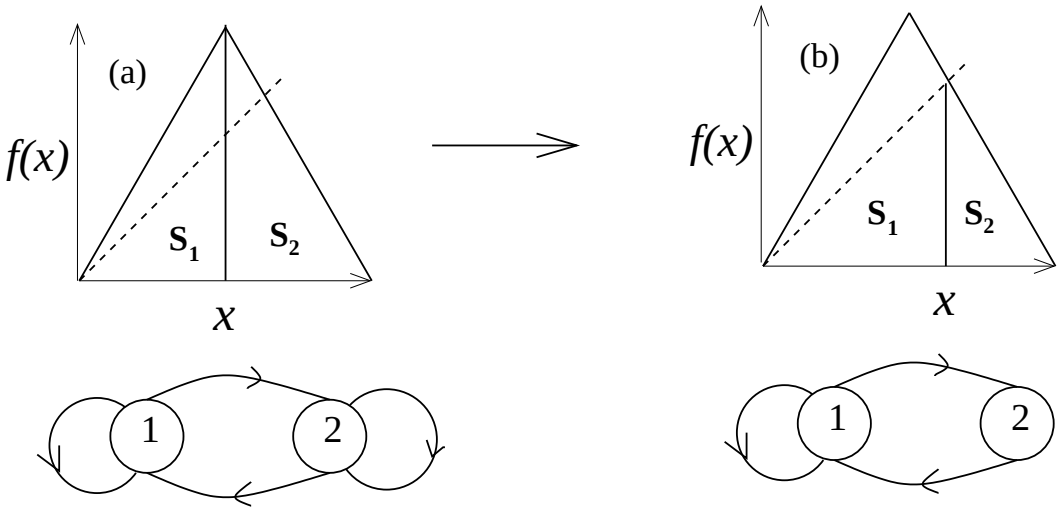


Fig. 1. The figure shows two different partition for the tent map (10). Subfigure (a) shows the generating partition, and the corresponding transition possibilities. (b) shows the partition that gives forbidden transitions (transition $2 \rightarrow 2$ is absent).

where $\overline{P(i,j)} = \frac{1}{m}\sum_k P_k^0(i,j)$ is calculated at $\varepsilon = 0$ and $k = 1, \ldots\ldots$ are $m$ different sets of random initial conditions drawn from the invariant measure of dynamics at the node. Note that $\delta^2$ is calculated by using only single node dynamics, whereas calculation of $\sigma^2$ involves all the dynamics of all the nodes. Further we will show that our symbolic measure based on the transition probabilities calculated for a single node is sufficient to detect global synchrony.

### *5.2 Tent Map*

The tent map is

$$f(x) = (1 - 2|x - \frac{1}{2}|). \tag{10}$$

Its stationary density on [0,1] is the uniform density, $p(x) \equiv 1$. If we take the generating partition [14], which is simply a partition of $[0, 1]$ with dividing point $l_p = 1/2$ [13], then the above tent map and a random sequence from a uniform distribution give equal Kolmogorov-Sinai (KS) entropy [19]. For this partition the iteration takes a trajectory to the left or right set of the partition with equal probabilities. As we shift the partition from $l_p = 1/2$, the transition probabilities remain no more the same and for $l_p = 2/3$, i.e., $S_1 = [0, l_p], S_2 = (l_p, 1]$, the transition $2 \rightarrow 2$ does not occur (see figure 1). Note that for this partition the difference between the permutation entropy of the tent map and the corresponding random system is maximal. As the partition point is moved further to the right in the range $a/(a + 1) \leq l_p < 1$, the transition remains forbidden, but the difference between entropies decreases, reaching zero at $l_p = 1$. The implication is that a longer time series

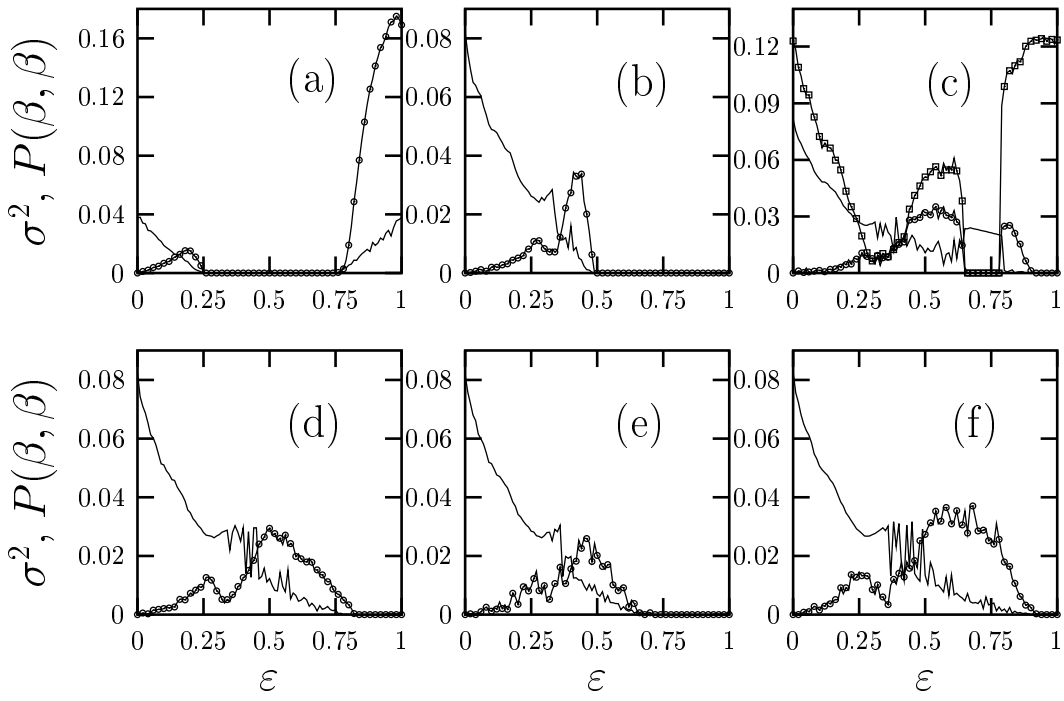


Fig. 2. Detection of synchronization in various networks of coupled maps. Figures are plotted for coupled tent maps (10). The networks consist of (a) two coupled maps, (b) a globally coupled network of size 50, (c) a small-world network of size 100 and average degree 30, (d) a scale-free network of size 100 and average degree 15, (e) a scale-free network of size 200 and average degree 10, and (f) a random network of size 200 and average degree 8. The horizontal axis is the coupling strength, and the vertical axis gives the synchronization measure $\sigma^2$ (–) for the whole network, as well as the transition probability $P(\beta,\beta)$ ($\circ$) calculated using a scalar time series fro m a randomly selected node. In all cases, the synchronization region ($\sigma^2 = 0$) coincides with the region where $P(\beta,\beta) = 0$ and the other transition probabilities are nonzero, which is the situation for the uncoupled map. Note that in subfigure (c) there is an interval of $\varepsilon$ roughly between 0.65 and 0.8 such that $P(\beta,\beta) = 0$, but there is no synchronization as $P(\alpha,\alpha)$ (shown by $\square$) is also zero here, unlike the case for the isolated tent map.

would now be needed as the observed occurrence of the symbol 2 becomes less frequent. Hence, the optimal partition would be the one for which the self-avoiding set $S_2$ is largest. Note that the choice of $l_p$ in the range $(1/2, a/(a+1))$ gives a non-generating partition, but has no two-symbol forbidden sequences. Although some longer sequences may be forbidden, their detection requires longer time series and more computational effort. For numerical calculations we use a slightly modified definition of the symbolic dynamics: To two consecutive measurements $x_t x_{t+1}$ we assign the symbol $\alpha$ if $x_{t+1} \geq x_t$ and the symbol $\beta$ otherwise [20]. This is equivalent to the symbol sequences defined by the sets $S_1, S_2$ because of the specific partition point $x^*$; thus the transition $\beta \to \beta$ does not occur for the single tent map. The advantage of using this definition of $\alpha, \beta$ is that one only needs to check increases and decreases in

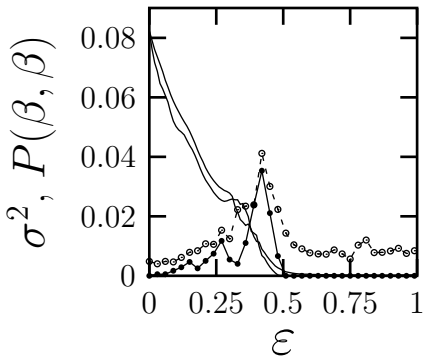


Fig. 3. Figure is plotted for globally connected networks with $N = 50$ and shows $P(\beta, \beta)$ for Gaussian noise with strength 2% (•) and 5% (◦).

the measured signal, which adds more robustness in case the fixed point is not precisely known. We evolve (6) starting from random initial conditions and estimate the transition probabilities using time series of length $\tau = 1000$ from a randomly selected node. Note that the length of the time series is much shorter than would be required by standard time-series methods which use embedding to reconstruct the phase space for large networks [21]. In our case, however, the length of the series is independent of the network size. We estimate the transition probability $P(i, j)$ ($i, j$ being $\alpha, \beta$) as given by Eq. (8). Synchronization is signalled when the variance of variables over the network $\sigma^2$ drops to zero. Fig. 2 summarizes the results. It is seen in all cases that the region for synchronization exactly coincides with the range for which $P(\beta, \beta)$ is zero (and other transition probabilities are nonzero; see subfigure (c)). Hence, regardless of network topology and size, both synchronized and unsynchronized behavior of the network can be accurately detected over the whole range of coupling strengths using only measurements from an arbitrarily selected node. The method is robust against external noise. Figure (3) plots $P(\beta, \beta)$ when the measurements are taken in the noisy environment.

For higher dynamical systems, for example Hénon maps and Lorenz attractor, finding optimal partitions corresponding to the maximal permutation entropy difference may be more difficult, but the method works for any non-generating partition and global synchrony is detected by comparing all the transition probabilities measured from a time series of an arbitrary node with those of the isolated function.

### *5.3 Hénon Map*

In this section we apply our method to coupled Hénon maps. The Hénon map is a two-dimensional map given by [22],

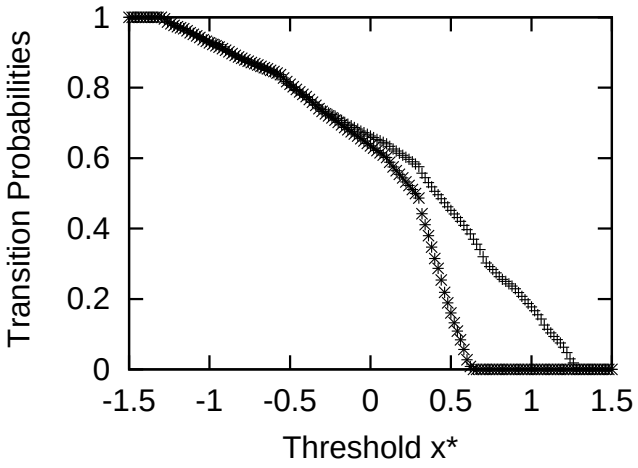


Fig. 4. Figures plots $P(\beta)(+)$ and $P(\beta,\beta)(*)$ as the function of the partition point $x*$ . The threshold is the point where $P(\beta,\beta)$ sharply drops to zero.

$$x(t+1) = y(t) + 1 - ax(t)^2$$
$$y(t+1) = by(t).$$

When one introduces the possibility of a time delay, the above equation can be written as the scalar equation

$$x(t+1) = bx(t-1) + 1 - ax(t)^2. \tag{11}$$

For the parameters, we take the values $a = 1.4$ and $b = 0.3$, for which the Hénon map is known to have a chaotic attractor.

Symbolic dynamics is defined as earlier. We use the natural density defined by the data to choose a threshold. Figure (4) depicts how the the probabilities of observing a single symbol $\beta$ and the repeated sequence $\beta\beta$ change depending on the value of the threshold $x^*$. It can be seen that a choice of $x^*$ roughly in the range $(0.55, 1.20)$ would be useful, since it renders the sequence $\beta\beta$ very unlikely without constraining the occurrence of the symbol $\beta$. Note that it is immediate from their definitions that the probabilities $P(\beta)$ and $P(\beta,\beta)$ will be decreasing as functions of $x^*$, and will approach zero as $x^*$ increases; furthermore, $P(\beta) > P(\beta,\beta)$. It follows that one can find a threshold $x^*$ for which $P(\beta)$ is large compared to $P(\beta,\beta)$. Figure (4) shows the sharp decrease in $P(\beta,\beta)(*)$ at about $x^* \approx 0.6$, so we can take some value near 0.6 as the threshold, which would yield very small $P(\beta,\beta)$ and a large $P(\beta)$ at the same time. We evolve (6) starting from random initial conditions, with (11) as local dynamics, and estimate the transition probabilities $P(i,j)$ as discussed in the first section, using a time series of length $\tau = 1000$. At the globally synchronized state $x_i(t) = x_j(t)$; $\forall i,j,t$, with all nodes evolving according to the rule (11), the symbolic sequences measured from a node will be subject to the same constraints as that generated by (11).

Figure 5 plots the transition probabilities as a function of the coupling strength.

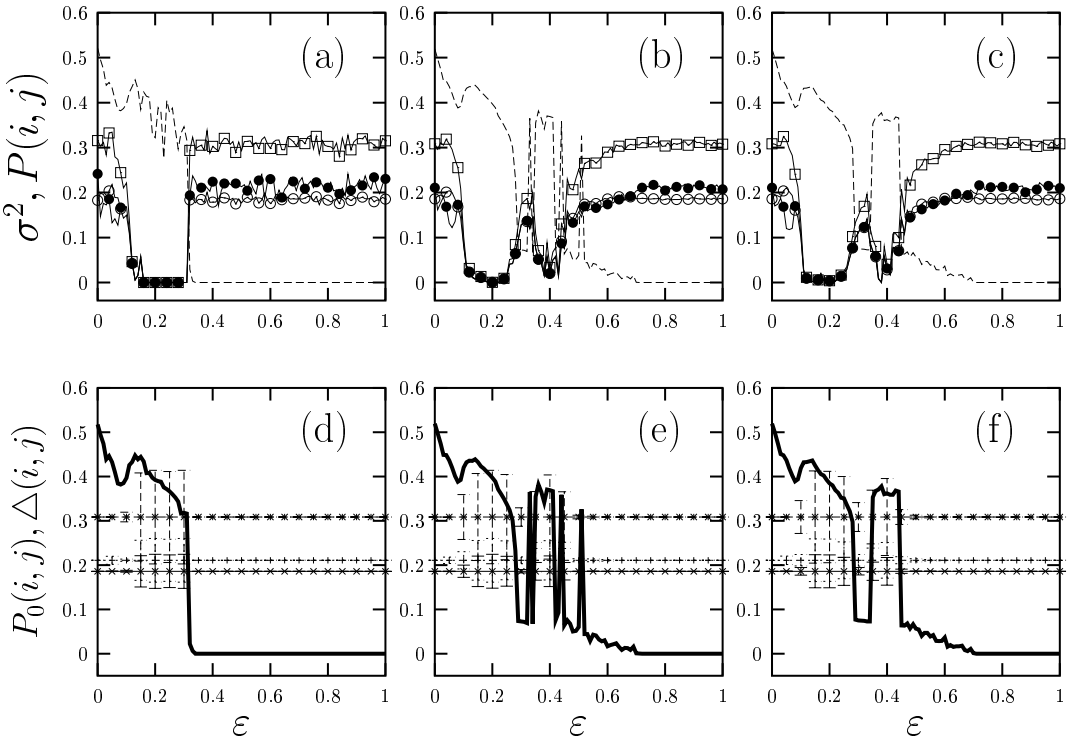


Fig. 5. The transition probability measure for coupled Hénon maps. The $x$-axis displays the coupling strength and the $y$-axis shows the different transition probabilities and the measure of synchronization $\sigma^2$. (a),(b) and (c) are plotted respectively for globally coupled network with $N = 50$, a random network and a scalefree network of size $N = 200$ and average degree 12. They plot transition probabilities for symbolic sequences of length 3, namely $P(\alpha, \alpha, \alpha)$ ($\Box$), $P(\alpha, \alpha, \beta)$ ($\bullet$), and $P(\beta, \alpha, \alpha)$ ($\circ$). Some of the transition probabilities are close to zero for most of the coupling strengths, so we do not plot these. The synchronized state is detected when all the transition probabilities are equal to those of the uncoupled map; i.e. the transition probabilities at zero coupling strength. (d), (e) and (f) are plotted for the above networks and they show the standard deviation $\sigma^2$ (solid thick line) and $\delta^2$ (vertical dashed line) for these three transition probabilities of an arbitrary selected node with respect to the transition probabilities of the uncoupled function ($P^0(i,j)$) (solid line), i.e for $\varepsilon = 0$. $\delta^2$ is calculated for 20 simulations for the dynamics with different sets of random initial conditions.

We consider the symbolic sequences of length two and three. For length two, we consider the transition probabilities $P(\alpha, \alpha)$ and $P(\beta, \beta)$. For sequences of length three we have 6 possible transitions, but some of them are very small (like $P(\beta, \beta, i)$ ), so we plot only those transition probabilities which vary with the couplings. It is clear from the figures that the synchronized state is easily detected by looking at the transition probabilities of any arbitrarily selected node. Whenever the transition probabilities are equal to the transition probabilities of the map (11), the network is globally synchronized. It is clear from subfigures (d),(e) and (f) that for the synchronized region (zero $\sigma^2$), the deviation of transition probabilities from the transition probabilities

of the uncoupled map (11) is also zero. Here, the deviation of $P(i,j)$ of any node is defined by Eq. (9). $k = 1, \ldots\ldots$ are $m$ different sets of random initial conditions taken between $-1.5$ and 1.5. In all the figures we get synchronization for larger coupling strengths, so the deviation is almost zero there, i.e. all transition probabilities match completely with those of the uncoupled map. Note that there are certain regions (small coupling strength range $\varepsilon < 0.15$) where the nodes do not get synchronized while the deviations are quite small. That is because for sufficiently small coupling strength, couplings do not affect the behaviour of the individual nodes very much, and so the transition probabilities also do not differ much from the uncoupled function. However, as we increase the coupling strength, the transition probabilities become dependent on the couplings. Still, if we look at the small coupling strength regions carefully we see that not all the deviations are small. For example, although the deviations of $P(\beta,\alpha,\alpha)$ (- - -) and $P(\alpha,\alpha,\beta)$ (-) are very small, the deviation in $P(\alpha,\alpha,\alpha)$ $(\ldots)$ is still large, whereas for the synchronized regime all deviations are very close to zero.

### *5.4 Lorenz Oscillator*

In this section we apply our method to coupled Lorenz oscillators. The following Lorenz oscillator gives chaotic attractor [22],

$$\begin{aligned} \dot{x} &= 10(y - x) \\ \dot{y} &= 28x - y - xz \\ \dot{z} &= -(8/3)z + xy \end{aligned} \tag{12}$$

We use only the $x$ variable to detect synchronization. This, in fact, again exhibits a principal feature of our approach, namely that we only need to evaluate partial information about the dynamics. Symbolic dynamics is defined as earlier, with $\triangle t = 0.2$ (section 2). We define the partition $(S_1, S_2)$ as $(a, x^*], [x^*, b)$, $a, b$ being the x-range for the Lorenz attractor. $x^*$ is obtained as earlier by checking the values of transition probabilities ($x(t) \in S_2$, and $x(t + \triangle t \in S_2)$, with varying $x^*$ (Fig. (6)). We evolve Eq. (5) starting from random initial conditions with (12) as local dynamics, and calculate the transition probabilities by using (8), from the $x$ time series of length $\tau = 1000$. Fig. (7) is plotted for the two coupled Lorenz oscillators. Global synchrony ($\dot{\mathbf{x}}_i(t) = \dot{\mathbf{x}}_j(t); \forall i, j, t$) is detected by comparing the transition probabilities measured from the $x$ time series of any randomly selected node with those of the $x$ time series of the uncoupled dynamics (12). $\sigma^2$ and $\delta^2$ are calculated as given in section 5.1. For $\varepsilon > 4.5$, the deviation of transition probabilities from those of the uncoupled case ($\varepsilon = 0$) is very small indicating the synchronization ($\sigma^2$ is also zero for this region).

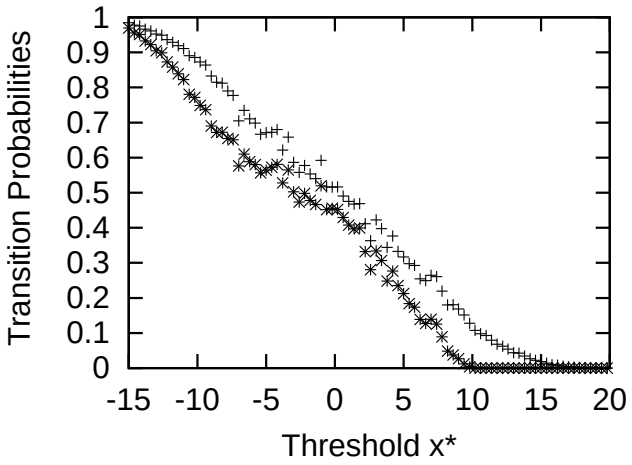


Fig. 6. Figure plots $P(\beta)(+)$ and $P(\beta,\beta)(*)$ for the Lorenz oscillator (Eq. (12)). The threshold for the partition is the point, $x^* \sim 10$, where $P(\beta,\beta)$ drops to zero (with $P(\beta)$ being non zero).

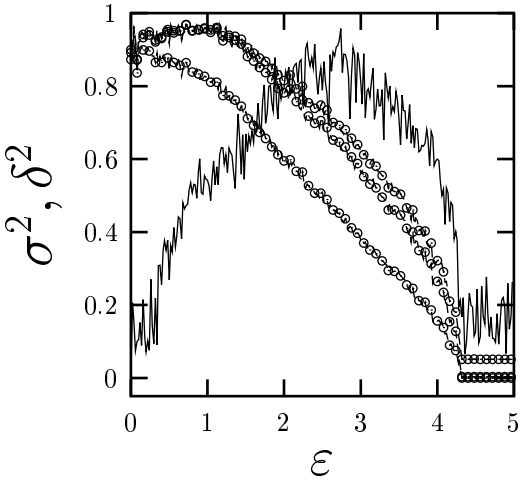


Fig. 7. The transition probability measure for coupled Lorenz oscillators. $\delta^2(--)$ (calculated by a scalar from a variable randomly selected node) and all the three $\sigma^2$'s corresponding to the $x, y$ and $z$ variables of the Lorenz oscillator are plotted as a function of the coupling strength.

## 6 Conclusion

We have presented a simple and effective method based on symbolic dynamics for the detection of synchronization in diffusively coupled networks. The method works by taking measurements from as few as one single node, and can utilize rather short sequences of measurements, and hence is computationally very fast.

The important point of the method is the following: our symbolic sequences are not drawn from the Markovian, that is, generating partitions which are the usual practice for symbolic dynamics. Rather, our symbolic sequences are

generated by non-generating partitions. The partitions which lead to the maximal difference between the chaotic dynamics and the corresponding random dynamics are the best ones for our purpose, and they prevent occurrence of certain symbol sequences related to the characteristics of the dynamics, so synchronization can be detected by checking for these forbidden symbolic sequences. However, for higher dimensional maps, finding the optimal partition (leading to maximal difference between the chaotic and corresponding random system) is difficult, but the method works for any non-generating partition and global synchrony is detected by comparing all the transition probabilities measured from a time series of an arbitrary node with those of the isolated function. So long as the synchronized dynamics is identical to the isolated dynamics, synchrony can be detected, and the fact that certain transition probabilities are exactly zero makes this procedure especially robust. The method is independent of the size and the connection architecture of the underlying network, and also robust against external noise.

## References


[1] A. T. Winfree, Science **298**, 2336 (2002); S Nadis, *Nature* (London) **421**, 780 (2003).

[2] A. Pikovsky, M. Rosenblum and J. Kurths, *Synchronisation : A Universal Concept in Nonlinear Dynamics* (Cambridge University Press, 2001).

[3] V. K. Vanag, I. R. Epstein, *Science* **294**, 835 (2001).

[4] P. R. Roelfsema, A K Engel, P. Konig, and W. Singer, *Nature* (London) **385**, 157 (1997).

[5] J. Engel, Jr. and T. A. Pedley (eds.), *Epilepsy: A Comprehensive Textbook* (Lippincott-Raven, Philadelphia, 1997).

[6] F. Mormann, T. Kreuz, R.G. Andrzejak, P. David, K. Lehnertz, C.E. Elger, *Epilepsy Res.* **53**, 173 (2003).

[7] W.-H. Kye, M. Choi, C.-M. Kim, and Y.-J. Park, *Phys. Rev. E* **71**, 045202(R) (2005).

[8] R. Agnihotri, K. Dutta, R. Bhushan, B. L. K. Somayajulu, *Earth Planet Sci. Lett.* **198**, 521 (2002).

[9] A. Stefanovska, H. Haken, P. V.E. McClintock, M. Hozic, F. Bajrovic, S. Ribaric, *Phys. Rev. Lett.* **85**, 4831 (2000).

[10] H. Kantz and T. Schreiber, *Nonlinear time series analysis* (Cambridge Univ. Press, 1997).

[11] S. Boccaletti, J. Kurths, G. Osipov, D. L. Valladare s and C. S. Zhou, *Physics Reports* **366**, 1 (2002)

[12] D. Lind and B. Marcus, *Symbolic dynamics and coding* (Cambridge Univ. Press, 1995).

[13] B.-Lin Hao and W.-M. Zheng, *Applied Symbolic Dynamics and Chaos* (World Scientific, 1998).

[14] D. J. Rudolph, *Fundamentals of Measurable Dynamics, Ergodic theory on Lebesgue spaces* (Clarendon Press, Oxford, 1990).

[15] E. M. Bollt, T. Stanford, Y.-C. Lai and K. Życzkowski, *Physica D* **154**, 259 (2001).

[16] C. Bandt and B. Pompe, *Phy. Rev. Lett.* **88** 174102 (2002).

[17] S. Jalan, F. M. Atay, and J. Jost (nlin.CD/0510057).

[18] S. Jalan, J. Jost and F. M. Atay, *Chaos* (in press).

[19] P. Grassberger and I. Procaccia, *Phys. Rev. A* **28**, 2591 (1983).

[20] Such a comparison between successive values of the variables has been introduced in [16] for the calculation of permutation entropy, and used in [23] for studying phase synchronization in coupled map networks. The first study [16] has shown that permutation entropy based on the comparison of $n$ successive values gives a good estimate of the KS entropy, and it matches the KS entropy for $n \to \infty$.

[21] J. D. Farmer and J. J. Sidorowich, *Phys. Rev. Lett.* **59**, 845 (1987); M. B. Kennel, R. Brown, and H. D. I. Abarbanel, *Phys. Rev. A* **45**, 3403-3411 (1992).

[22] A. J. Lichtenberg and M. A. Lieberman, *Regular and Chaotic Dynamics* (Springer-Verlag, 1983).

[23] S. Jalan and R. Amritkar, *Phys. Rev. Lett.* **90** 014101 (2003).

[24] P. Tass, M. Rosenblum, J. Weule, J. Kurths, A. Pikovsky, J. Volkmann, A. Schitzler and H. Freund, *Phys. Rev. Lett.* **81**, 3291 (1998).

[25] R. Q. Quironga, T Kreuz and P. Grassberger, *Phys. Rev. E* **66**, 041904 (2002).

[26] F. Takens, in *Dynamical Systems and Turbulence* (Warwick 1980), edited by D. A. Rand and L.-S. Young (Springer-Verlag, Berlin, 1980), Vol. 898, pp366-381.

[27] K. Kaneko, *Physica D* **34**, 1 (1989); Phys. Rev. Lett. **65** 1391 (1990) *Physica D* **41**, 137 ( 1990 ); *Physica D* **124**, 322 (1998).